

Realizing the quantum baker's map on an NMR quantum computer

Todd Brun* ^(a) and Rüdiger Schack† ^(b)

^(a) *Institute for Theoretical Physics,
University of California, Santa Barbara, CA 93106, USA*

^(b) *Department of Mathematics, Royal Holloway,
University of London, Egham, Surrey TW20 0EX, UK*

(17 December 1998)

Abstract

By numerically simulating an implementation of the quantum baker's map on an NMR quantum computer based on the molecule trichloroethylene, we demonstrate the feasibility of quantum chaos experiments on present-day quantum computers. We give detailed descriptions of proposed experiments that investigate (a) the rate of entropy increase due to decoherence and (b) the phenomenon of hypersensitivity to perturbation.

I. INTRODUCTION

The quantum baker's map [1,2] is a simple map invented for the theoretical investigation of quantum chaos. Its mathematical properties have been studied extensively, but no experimental quantum systems are known which embody it. Recently, one of us has shown that the quantum baker's map has a simple realization on a quantum computer [3]. In this paper, we present realistic numerical simulations of an NMR quantum computer [4–6] using three quantum bits (qubits) to explore the chaotic properties of the quantum baker's map.

In Section II we review the definition of the quantum baker's map and its qubit realization. We present a simple argument [7] showing that the quantum baker's map is equivalent to a shift map [8,9] on a string of qubits. This leads to the definition of a simplified quantum baker's map which we use in the later parts of this paper.

In Section III we review the 3-qubit NMR quantum computer based on the molecule trichloroethylene used in Ref. [10] and give the radio-frequency (RF) pulse sequence for the proton and carbon spins of the molecule implementing the quantum baker's map. Since

*Present address: Department of Physics, Carnegie Mellon University, Pittsburgh, PA 15213.
E-mail: tbrun@andrew.cmu.edu

†E-mail: r.schack@rhbnc.ac.uk

decoherence cannot be neglected for this experiment, we model the NMR system by a master equation of Lindblad form [11], including the Hamiltonian time evolution, the RF pulses, and phase noise due to the environment, using the actual experimental parameters.

Finally, in Section IV we propose two specific quantum chaos experiments. In both experiments, we compare the quantum baker's map with a trivial *regular* map. One experiment analyses the rate of increase of the von Neumann entropy due to decoherence [12,13], which is related to a quantum generalization of the Kolmogorov-Sinai (KS) entropy [8,14]. The other experiment examines whether the 3-qubit quantum baker's map is *hypersensitive to perturbation*. Hypersensitivity to perturbation is an information-theoretic criterion for classical and quantum chaos [15–18] which has been shown to be equivalent to a standard definition of classical chaos under general assumptions [16].

II. THE QUANTUM BAKER'S MAP AS A SHIFT MAP ON QUBITS

The classical baker's transformation [19], which maps the unit square $0 \leq q, p \leq 1$ onto itself, has a simple description in terms of its symbolic dynamics [20]. Each point in phase space is represented by a symbolic string $s = \cdots s_{-2}s_{-1}s_0.s_1s_2\cdots$ where $s_k = 0$ or 1. In the string s , the bits to the right of the dot are the binary expansion of the q coordinate, and the bits to the left of the dot, read backwards, are the binary expansion of the p coordinate. Written formally, s is identified with a point (q, p) in the unit square by setting $q = \sum_{k=1}^{\infty} s_k 2^{-k}$ and $p = \sum_{k=0}^{\infty} s_{-k} 2^{-k-1}$. The action of the baker's map on a symbolic string is given by the shift map U defined by $(Us)_k = s_{k+1}$, which means that, at each time step, the entire string is shifted one place to the left while the dot remains fixed. Geometrically, if q labels the horizontal direction and p labels the vertical, the baker's map on the unit square is equivalent to stretching the q direction and squeezing the p direction each by a factor of two, then stacking the right half on top of the left. The definition of the baker's map through its symbolic dynamics emphasizes its prototypical character for investigations of chaotic maps: A very large class of chaotic maps can be shown to be equivalent to shifts on symbolic strings [20]. Furthermore, it is shown below that the quantum baker's map is equivalent to a shift on a string of qubits.

To define the quantum baker's map [1], we quantize the unit square as in [2,21]. To represent the unit square in D -dimensional Hilbert space, we start with unitary “displacement” operators \hat{U} and \hat{V} , which produce displacements in the “momentum” and “position” directions, respectively, and which obey the commutation relation [21]

$$\hat{U}\hat{V} = \hat{V}\hat{U}\epsilon, \quad (1)$$

where $\epsilon^D = 1$. We choose $\epsilon = e^{2\pi i/D}$. We further assume that $\hat{V}^D = \hat{U}^D = 1$, i.e., periodic boundary conditions. It follows [2,21] that the operators \hat{U} and \hat{V} can be written as

$$\hat{U} = e^{2\pi i\hat{q}} \quad \text{and} \quad \hat{V} = e^{-2\pi i\hat{p}}. \quad (2)$$

The “position” and “momentum” operators \hat{q} and \hat{p} both have eigenvalues j/D , $j = 0, \dots, D-1$.

In the following, we restrict the discussion to the case $D = 2^N$, i.e., the dimension of Hilbert space is a power of two. For consistency of units, we let the quantum scale on “phase

space" be $2\pi\hbar = 1/D = 2^{-N}$. A transformation between the position basis $\{|q_j\rangle\}$ and the momentum basis $\{|p_j\rangle\}$ is effected by the discrete Fourier transform F_N , defined by

$$F_N|q_j\rangle = |p_j\rangle = \sqrt{2\pi\hbar} \sum_{k=0}^{D-1} e^{ip_j q_k/\hbar} |q_k\rangle = \frac{1}{\sqrt{D}} \sum_{k=0}^{D-1} e^{2\pi i k j/D} |q_k\rangle. \quad (3)$$

The $D = 2^N$ dimensional Hilbert space modeling the unit square can be realized as the product space of N qubits (i.e. N two-state systems) in such a way that

$$|q_j\rangle = |a_{N-1}\rangle \otimes |a_{N-2}\rangle \otimes \cdots \otimes |a_0\rangle, \quad (4)$$

where $j = \sum a_k 2^k$, $a_k \in \{0, 1\}$ ($k = 0, \dots, N-1$), and where each qubit has basis states $|0\rangle$ and $|1\rangle$. It follows that, written as a binary expansion, $q_j = 0.a_{N-1} \dots a_0 \equiv a_{N-1}2^{-1} + \cdots + a_02^{-N}$.

There is no unique way to quantize a classical map. Here we adopt the quantized baker's map introduced by Balazs and Voros [1], which can be written as [3]

$$T = F_N^{-1}(I \otimes F_{N-1}), \quad (5)$$

where F_{N-1} acts on the $N-1$ least significant qubits, and I is the identity operator acting on the most significant qubit. Saraceno [2] has introduced a quantum baker's map with stronger symmetry properties by using antiperiodic boundary conditions, but in this article we restrict the discussion to periodic boundary conditions as used in [1]. It is straightforward to adapt the discussion in this paper to Saraceno's version of the map [22].

Note that [23]

$$\begin{aligned} |\psi\rangle &\equiv F_N^{-1}|a_{N-1}\rangle \otimes \cdots \otimes |a_0\rangle \\ &= (|0\rangle + e^{-2\pi i(0.a_0)}|1\rangle) \otimes \cdots \otimes (|0\rangle + e^{-2\pi i(0.a_{N-2} \dots a_0)}|1\rangle) \otimes (|0\rangle + e^{-2\pi i(0.a_{N-1} \dots a_0)}|1\rangle) \end{aligned} \quad (6)$$

and

$$\begin{aligned} |\phi\rangle &\equiv (I \otimes F_{N-1})^{-1}|a_{N-1}\rangle \otimes \cdots \otimes |a_0\rangle \\ &= |a_{N-1}\rangle \otimes (|0\rangle + e^{-2\pi i(0.a_0)}|1\rangle) \otimes \cdots \otimes (|0\rangle + e^{-2\pi i(0.a_{N-2} \dots a_0)}|1\rangle). \end{aligned} \quad (7)$$

As $|\psi\rangle = T|\phi\rangle$, T can be seen to perform a shift of the qubits [7], in which the most significant qubit of the argument $|\phi\rangle$ is transformed in a way that depends on all the other qubits, becoming the least significant qubit of the image $|\psi\rangle$. The quantum baker's map (5) is thus equivalent to a shift map on a quantum spin chain [8], in analogy to the symbolic dynamics for the classical baker's map.

The quantum baker's map can be realized using the following basic unitary operations or *quantum gates*: the Hadamard transform gate A_m acting on the m th qubit and defined in the basis $\{|0\rangle, |1\rangle\}$ by the matrix

$$A_m = \frac{1}{\sqrt{2}} \begin{pmatrix} 1 & 1 \\ 1 & -1 \end{pmatrix}, \quad (8)$$

and the phase gate $B_{mn}(\theta)$ operating on the m th and n th qubits and defined by

$$B_{mn}(\theta) |a_{L-1}\rangle \otimes \cdots \otimes |a_0\rangle = e^{i\phi_{a_m a_n}} |a_{L-1}\rangle \otimes \cdots \otimes |a_0\rangle, \quad (9)$$

where

$$\phi_{a_m a_n} = \begin{cases} \theta & \text{if } a_m = a_n = 1, \\ 0 & \text{otherwise.} \end{cases} \quad (10)$$

In addition we define the gate S_{mn} which swaps the qubits m and n .

In $D = 8 = 2^3$ dimensional Hilbert space, one iteration of the quantum baker's map is performed by the sequence of gates

$$T = S_{02} A_0 B_{01}^\dagger(\pi/2) B_{02}^\dagger(\pi/4) A_1 B_{12}^\dagger(\pi/2) A_2 S_{01} A_0 B_{01}(\pi/2) A_1. \quad (11)$$

The corresponding pulse sequence on the NMR computer is quite long and complicated (see Section III and the Appendix). Therefore we introduce a simplified version, $T_{\mathcal{M}}$, of the quantum baker's map [7]. $T_{\mathcal{M}}$ maps each of the states

$$\begin{aligned} & |a_{N-1}\rangle \otimes (|0\rangle + e^{-2\pi i(0.a_0 \dots a_{N-2})}|1\rangle) \otimes (|0\rangle + e^{-2\pi i(0.a_1 \dots a_{N-2})}|1\rangle) \\ & \otimes \dots \otimes (|0\rangle + e^{-2\pi i(0.a_{N-2})}|1\rangle) \end{aligned} \quad (12)$$

to

$$\begin{aligned} & (|0\rangle + e^{-2\pi i(0.a_0 \dots a_{N-2} a_{N-1})}|1\rangle) \otimes (|0\rangle + e^{-2\pi i(0.a_1 \dots a_{N-2} a_{N-1})}|1\rangle) \\ & \otimes \dots \otimes (|0\rangle + e^{-2\pi i(0.a_{N-1})}|1\rangle), \end{aligned} \quad (13)$$

and is thus equivalent to $N - 1$ a_{N-1} -controlled rotations, a Hadamard transform on the most significant qubit, and then a cyclic shift of the qubits. In $D = 8 = 2^3$ dimensional Hilbert space, one iteration of the map $T_{\mathcal{M}}$ is performed by the much shorter sequence of gates

$$T_{\mathcal{M}} = S_{01} S_{02} A_0 B_{02}^\dagger(\pi/4) B_{01}^\dagger(\pi/2). \quad (14)$$

Like the quantum baker's map T , the simplified map $T_{\mathcal{M}}$ is a shift on a string of qubits, although $T_{\mathcal{M}}$ leads to different phase relations between the qubits. The two maps can thus be expected to have similar chaotic behavior. We have confirmed this expectation by comparing the numerical results of Section IV with simulations of the full quantum baker's map T [24]; these simulations are not included here because, unlike the results of the present paper, they are based on unrealistic assumptions for the experimental parameters.

III. IMPLEMENTATION ON AN NMR QUANTUM COMPUTER

A. The system and its Hamiltonian

We choose for our physical system the molecule trichloroethylene (Fig. 1), in which the nuclear spins of the hydrogen and two carbons serve as our qubits. These spins weakly interact with each other on a single molecule, but are effectively shielded from the environment by rapid tumbling. The molecules are placed in a strong, uniform magnetic field and subjected to RF pulses at various frequencies.

We denote by \hat{X} , \hat{Y} , and \hat{Z} the σ_x , σ_y , and σ_z Pauli matrices, respectively, and indicate with a subscript (e.g., \hat{X}_H) to which spin they apply. The Hamiltonian of the three spins in the interaction picture is

$$\hat{H} = \frac{j_1}{4}\hat{Z}_H\hat{Z}_{C_1} + \frac{j_2}{4}(\hat{X}_{C_1}\hat{X}_{C_2} + \hat{Y}_{C_1}\hat{Y}_{C_2} + \hat{Z}_{C_1}\hat{Z}_{C_2}) + \frac{j_3}{4}\hat{Z}_H\hat{Z}_{C_2} + \frac{\delta}{2}\hat{Z}_{C_2}, \quad (15)$$

where $j_1 \approx 203$ Hz, $j_2 \approx 102$ Hz, $j_3 \approx 10$ Hz and $\delta \approx -905$ Hz [25].

It is convenient to approximate the interaction term between the two carbons by $(j_2/4)\hat{Z}_{C_1}\hat{Z}_{C_2}$, omitting the $\hat{X}\hat{X}$ and $\hat{Y}\hat{Y}$ terms. This approximation is somewhat difficult to justify, but greatly simplifies the description of the quantum gates. Generally, it works well if the spin precession frequency of two spins differs by an amount large compared to the spin coupling j [26]. This is true between H and C_1 (where the approximation has already been made), but only borderline between C_1 and C_2 . The approximate Hamiltonian is then

$$\hat{H}' = \frac{j_1}{4}\hat{Z}_H\hat{Z}_{C_1} + \frac{j_2}{4}\hat{Z}_{C_1}\hat{Z}_{C_2} + \frac{j_3}{4}\hat{Z}_H\hat{Z}_{C_2} + \frac{\delta}{2}\hat{Z}_{C_2}, \quad (16)$$

For our numerical simulations, we will assume the form \hat{H}' of the Hamiltonian, but we have checked the dependence of our results on this approximation. Whenever the data curves obtained using \hat{H} differ from those obtained using \hat{H}' , we present both curves.

Since j_3 is small compared to the other terms in the Hamiltonian, it may be safely neglected for the design of the pulse sequences (see below). The j_3 term cannot be neglected, however, in the simulation of the full dynamics including noise [see Eq. (34)], since it is of the same order of magnitude as the leading noise terms. Thus, for the discussion of the pulse sequences only, we will assume the following, further simplified form of the Hamiltonian,

$$\hat{H}'' = \frac{j_1}{4}\hat{Z}_H\hat{Z}_{C_1} + \frac{j_2}{4}\hat{Z}_{C_1}\hat{Z}_{C_2} + \frac{\delta}{2}\hat{Z}_{C_2}. \quad (17)$$

In addition to these interactions, we can apply RF pulses which rotate the nuclear spins about the x and y axes. By controlling the pulse frequencies, these can be selectively applied to single spins (soft pulses), or to two or three spins at once (hard pulses) [6]. In our simulations, we use instantaneous pulses, i.e., we assume that the duration of the pulses is very short compared to the timescale of the Hamiltonian \hat{H}'' . This assumption is only marginally satisfied for soft pulses. The general conclusions of this paper, however, are not affected by this approximation, since they do not depend on the precise form of the implemented map.

For the purposes of our simulations we also assume that the RF pulses are timed with perfect accuracy. Unfortunately, this is not the case in experiment, where one can expect errors of 1–10% or even higher [27]. This is an additional complication, which muddies the argument without changing its basic conclusions; hence we neglect it.

The general form of a quantum algorithm in an NMR computer is a sequence of pulses, causing rotations of the individual bits, interspersed by precisely-timed delays during which the undriven Hamiltonian couples the neighboring spins [4–6]. In describing such a sequence, $X(\theta)$ denotes a rotation about the x axis by an angle θ . This is equivalent to multiplying the state by the operator $\exp(i\theta\hat{X}/2)$. $Y(\theta)$ denotes a similar rotation about the y axis.

$U(t)$ indicates a delay of duration t , during which the Hamiltonian \hat{H}'' acts. A sequence is to be read from right to left, i.e., the rightmost operation is performed first. In this way, composition of the operations follows the same sense as operator multiplication. Subscripts indicate which spin is acted on.

The basic gates which form the algorithm are constructed from these simple pulse sequences, as we will show below. Note that in all cases we neglect the overall phase of the state. Thus, two gates will be considered equivalent if they agree up to an overall phase.

B. One-bit gates

We are already equipped with two families of one-bit gates, the x and y rotations. Two other useful gates, however, are lacking: z rotations and Hadamard transforms. Fortunately, in both cases these can be built from sequences of simple pulses [28].

Rotations about z can be constructed from a sequence of three x and y rotations [29]:

$$Z(\theta) = X(-\pi/2)Y(\theta)X(\pi/2). \quad (18)$$

In fact, there are several such combinations which can be used to produce a z rotation. As gates are put together in a quantum algorithm, it is often useful to choose their precise form so that a certain number of pulses combine or even cancel out, hence simplifying the overall sequence. Thus, we can write any of the following:

$$\begin{aligned} Z(\theta) &= X(-\pi/2)Y(\theta)X(\pi/2) \\ &= X(\pi/2)Y(-\theta)X(-\pi/2) \\ &= Y(\pi/2)X(\theta)Y(-\pi/2) \\ &= Y(-\pi/2)X(-\theta)Y(\pi/2), \end{aligned} \quad (19)$$

as convenient in constructing the algorithm.

We also need the Hadamard transform A defined in (8), which can be effected by a pair of x and y rotations

$$\begin{aligned} A &= Y(\pi/2)X(\pi) \\ &= X(-\pi)Y(-\pi/2). \end{aligned} \quad (20)$$

Again, the form is chosen to simplify the sequence as much as possible.

C. Two-bit gates

Given the large family of one-bit gates to choose from, we need only a limited selection of two-bit gates. This is good, because we have only a limited selection to choose from. To build our algorithm, all we need is the phase gate $B_{ij}(\theta)$ defined in equation (9) which couples pairs of bits. The phase gate between bits i and j can be decomposed into

$$B_{ij}(\theta) = \exp(i\theta\hat{Z}_i/4) \exp(i\theta\hat{Z}_j/4) \exp(i\theta\hat{Z}_i\hat{Z}_j/4). \quad (21)$$

The $\hat{Z}_i\hat{Z}_j$ term is the critical one. Transformations of that type are produced by the Hamiltonian evolution (17). However, this includes unwanted additional terms. We can effectively eliminate these terms by the technique of *refocusing*, in which we “undo” the evolution of all but the selected term in the Hamiltonian [29,4,5]. Because of the anticommutation of the Pauli matrices,

$$\hat{X}_i \exp(i\theta\hat{Z}_i\hat{Z}_j) = \exp(-i\theta\hat{Z}_i\hat{Z}_j)\hat{X}_i, \quad i \neq j. \quad (22)$$

Thus, if we stick an x pulse in the middle of a period of Hamiltonian evolution, it can effectively remove the unwanted terms.

$$\begin{aligned} \hat{X}_H \exp(-i\hat{H}''\tau)\hat{X}_H \exp(-i\hat{H}''\tau) &= \exp(-i\tau j_2 \hat{Z}_{C_1} \hat{Z}_{C_2}/2 - i\tau \delta \hat{Z}_{C_2}) \\ \hat{X}_{C_2} \exp(-i\hat{H}''\tau)\hat{X}_{C_2} \exp(-i\hat{H}''\tau) &= \exp(-i\tau j_1 \hat{Z}_H \hat{Z}_{C_1}/2). \end{aligned} \quad (23)$$

We use this to build phase gates between neighboring spins.

$$B_{C_1H}(-\theta) = Z_H(-\theta/2)Z_{C_1}(-\theta/2)X_{C_2}(\pi)U(\tau)X_{C_2}(\pi)U(\tau), \quad (24)$$

where $\tau = \theta/2j_1$. Note that one can use y rotations instead of x , and shuffle the order of these operations; also, one can choose any of the expressions (19) for the z rotations. A very similar expression applies for $B_{C_1C_2}$, using X_H instead of X_{C_2} , but we must also include an additional Z_{C_2} rotation to undo the effects of the $\delta\hat{Z}_{C_2}/2$ term in the Hamiltonian.

While the phase gate is useful in itself, it can also be used to produce the *controlled-not* (CNOT) gate by nesting it between two Hadamard transforms, $C_{ij} = A_i B_{ij}(\pi) A_i$.

D. Swaps

A disadvantage of the Hamiltonian (17) is that it only couples neighboring spins. If we wish to perform a two-bit gate on H and C_2 , we have to swap one of them with the central spin, C_1 , using the swap gates S_{C_1H} and $S_{C_1C_2}$.

Swaps can be built from a sequence of CNOT gates:

$$S_{ij} = C_{ij}C_{ji}C_{ij}. \quad (25)$$

Each CNOT is composed of a phase gate and two Hadamard transforms, as shown above, and the phase gates in turn are built out of precisely timed Hamiltonian evolution interspersed with RF pulses. Thus, to swap the H and C_1 spins requires the sequence

$$\begin{aligned} S_{C_1H} &= A_H Z_H(\pi/2)Z_{C_1}(\pi/2)X_{C_2}U(\tau)X_{C_2}U(\tau)A_H A_{C_1} Z_H(\pi/2)Z_{C_1}(\pi/2)X_{C_2}U(\tau)X_{C_2}U(\tau) \\ &\times A_H A_{C_1} Z_H(\pi/2)Z_{C_1}(\pi/2)X_{C_2}U(\tau)X_{C_2}U(\tau)A_H, \end{aligned} \quad (26)$$

where $\tau = \pi/2j_1$. The C_1 - C_2 swap is similar. Since each of the Hadamard transforms and z rotations is itself a product of several RF pulses, we see that the swap gate is quite large and complicated. What is more, the three phase gates take considerable time, allowing the system to be affected by decoherence. The number of RF pulses can be somewhat reduced by carefully choosing the expressions for the Hadamard and z gates to cancel as many pulses as possible, but there is nothing to be done about the time for the phase gates.

It is clearly to our advantage to perform as few swaps as possible. We follow this precept in designing the map $T_{\mathcal{M}}$. As it is, more than half the time of the algorithm is spent in swapping.

E. The map $T_{\mathcal{M}}$

In section II we defined a simplified version of the quantum baker's map, which in the three-bit case is given by (14). This map has two important traits. First, all of its two-bit gates involve bit 0. Second, the two swap gates perform a cyclic shift of the bits, $0 \rightarrow 2 \rightarrow 1 \rightarrow 0$.

Since we can only couple neighboring spins, it makes the most sense to make 0 the central bit, C_1 . We can then identify bit 1 with H and bit 2 with C_2 . In terms of the physical bits, then, the map becomes

$$T_{\mathcal{M}} = S_{C_1 H} S_{C_1 C_2} A_{C_1} B_{C_1 C_2}(-\pi/4) B_{C_1 H}(-\pi/2). \quad (27)$$

Further examination reveals that the $S_{C_1 C_2}$ is unnecessary. The shift $1 \rightarrow 0$ is necessary in order to keep bit 0 in the central position. The labeling of bits 1 and 2, however, is arbitrary. We could just have easily identified bit 1 with C_2 and bit 2 with H . Thus, we need not perform an actual physical swap gate here; a mental re-labeling of the bits is sufficient.

This means that the labeling of the bits will switch back and forth between even and odd iterations of the map. Thus, the physical realization of the map will also differ between even and odd steps. We therefore have two alternating sequences,

$$\begin{aligned} T_{\text{odd}} &= S_{C_1 H} A_{C_1} B_{C_1 C_2}(-\pi/4) B_{C_1 H}(-\pi/2) \\ T_{\text{even}} &= S_{C_1 C_2} A_{C_1} B_{C_1 H}(-\pi/4) B_{C_1 C_2}(-\pi/2). \end{aligned} \quad (28)$$

Each of these gates represents a given series of RF pulses and delays. By choosing the form of the z rotations and A gates carefully, and ordering the operators for the B gates appropriately, a certain amount of cancellation is possible, simplifying the sequence somewhat. In this way we arrive at the following sequence of elementary pulses:

$$\begin{aligned} T_{\text{odd}} &= X_H(-3\pi/2) Y_H(-\pi/2) Y_{C_1}(\pi/2) X_{C_1}(-\pi/2) Y_{C_1}(-\pi/2) U(\tau_1) X_{C_2}(\pi) U(\tau_1) X_H(-3\pi/2) \\ &\quad \times X_{C_1}(-3\pi/2) Y_H(-\pi/2) Y_{C_1}(-\pi/2) U(\tau_1) X_{C_2}(\pi) U(\tau_1) X_H(-3\pi/2) X_{C_1}(-3\pi/2) \\ &\quad \times Y_H(-\pi/2) Y_{C_1}(-\pi/2) U(\tau_1) X_{C_2}(\pi) U(\tau_1) X_{C_2}(\pi/2) Y_{C_2}(\delta\tau_1 - \pi/8) \\ &\quad \times X_{C_2}(\pi/2) X_H(-5\pi/4) Y_H(-\pi/2) X_{C_1}(-11\pi/8) Y_{C_1}(-\pi/2) U(\tau_1), \end{aligned} \quad (29)$$

where $\tau_1 = \pi/2j_1$. Note that because $j_1 \approx 2j_2$ we can combine the two B gates into a single time delay for T_{odd} .

This unfortunately works in exactly the wrong direction for T_{even} , which consequently makes the sequence somewhat longer and more complex:

$$\begin{aligned} T_{\text{even}} &= X_{C_2}(2\delta\tau_2 - 3\pi/2) Y_{C_2}(\pi/2) Y_{C_1}(\pi/2) X_{C_1}(\pi/2) Y_{C_1}(\pi/2) U(\tau_2) X_H(\pi) \\ &\quad \times U(\tau_2) X_{C_1}(-3\pi/2) X_{C_2}(2\delta\tau_2 - 3\pi/2) Y_{C_1}(-\pi/2) Y_{C_2}(-\pi/2) U(\tau_2) X_{C_1}(\pi) U(\tau_2) \\ &\quad \times X_{C_1}(-3\pi/2) X_{C_2}(2\delta\tau_2 - 3\pi/2) Y_{C_1}(-\pi/2) Y_{C_2}(-\pi/2) U(\tau_2) X_{C_1}(\pi) U(\tau_2) \\ &\quad \times X_H(\pi/2) Y_H(-\pi/8) X_H(-\pi/2) X_{C_2}(4\delta\tau_3 - 5\pi/4) Y_{C_2}(-\pi/2) X_{C_1}(-11\pi/8) \\ &\quad \times Y_{C_1}(-\pi/2) U(3\tau_3/2) X_H(\pi) U(5\tau_3/2), \end{aligned} \quad (30)$$

where $\tau_2 = 2\tau_1$ and $\tau_3 = \tau_1/2$. (Recall that these sequences should be read from right to left.) The total delay time for T_{odd} is $7\tau_1$, while the delay time for T_{even} is $14\tau_1$, taking twice as long. Thus, intrinsic noise affects the system more during even steps than odd ones.

F. The regular map $T_{\mathcal{R}}$

Having defined a quantized version of a classically chaotic map, we need to define a regular map for comparison. This map should take the same time per iteration as the map $T_{\mathcal{M}}$, on average, so that it is affected equally by the intrinsic noise.

The simplest possibility would be a map that does essentially nothing. This implies that the effects of the Hamiltonian in coupling the spins must be suppressed. We do this by refocusing, as described above. Consider the sequence

$$T_{\mathcal{R}} = X_{C_1}(\pi)U(\tau_4)X_{C_1}(\pi)U(\tau_4)X_{C_1}(\pi)U(\tau_4)X_{C_1}(\pi)U(\tau_4)X_{C_1}(\pi)U(\tau_4)X_{C_1}(\pi)U(\tau_4) \times X_{C_1}(\pi)U(\tau_4)X_{C_1}(\pi)U(\tau_4). \quad (31)$$

The x rotations flip the sign of all terms containing \hat{Z}_{C_1} in the Hamiltonian, so that the effects of these terms cancel out. That is, all but the $\delta\hat{Z}_{C_2}/2$ term of (17) are effectively eliminated:

$$X_{C_1}(\pi)U(\tau)X_{C_1}(\pi)U(\tau) \approx \exp(-i\delta\tau\hat{Z}_{C_2}). \quad (32)$$

Thus, we see that

$$T_{\mathcal{R}} \approx \exp(-4i\delta\tau_4\hat{Z}_{C_2}). \quad (33)$$

By performing an appropriate z rotation at the end we could eliminate this cumulative rotation of the C_2 spin, but as it makes no difference to the regularity of the map we leave it unaltered for simplicity. The total time $8\tau_4$ should equal the average iteration time of the map $T_{\mathcal{M}}$, so $\tau_4 = 21\tau_1/16 = 21\pi/32j_1$.

G. Noise and the master equation

While the nuclear spins are fairly well isolated, this isolation is not perfect. Interactions with the external environment cause the spins to deviate from strict Hamiltonian evolution, a deviation which becomes increasingly important as the length of the NMR calculation increases.

The effects of the environment are described by two timescales T_1 and T_2 [30]. T_1 is the timescale on which the spins relax to the thermal state. T_2 is the timescale of phase decoherence, the result of the spins becoming correlated with the state of the environment and hence going from a superposition of states to a statistical mixture. For the molecule trichloroethylene, T_1 exceeds T_2 by an order of magnitude, and can be safely neglected for this problem.

We model the effect of T_2 by replacing the state vector $|\psi\rangle$ with a density matrix ρ and the Schrödinger equation with a Markovian master equation in Lindblad form [11],

$$\frac{d\rho}{dt} = -i[\hat{H}', \rho] + \frac{1}{2} \sum_k 2 \left(\hat{L}_k \rho \hat{L}_k^\dagger - \hat{L}_k^\dagger \hat{L}_k \rho - \rho \hat{L}_k^\dagger \hat{L}_k \right), \quad (34)$$

where \hat{H}' is the Hamiltonian (16) and the \hat{L}_k are a set of operators chosen to model the effects of decoherence. The simplest choice of \hat{L}_k 's which capture the essential physics are proportional to the \hat{Z} operator for each of the three spins:

$$\begin{aligned}
\hat{L}_1 &= \sqrt{\Gamma_H} \hat{Z}_H, \\
\hat{L}_2 &= \sqrt{\Gamma_{C_1}} \hat{Z}_{C_1}, \\
\hat{L}_3 &= \sqrt{\Gamma_{C_2}} \hat{Z}_{C_2}.
\end{aligned}
\tag{35}$$

The decay rate Γ is proportional to $1/T_2$ for each spin.

Using quantum trajectory techniques [31,32], we can solve the above master equation numerically for various choices of T_2 and various initial states. We treat the RF pulses as instantaneous unitary transformations, just as before. They interrupt the continuous master equation evolution given above.

IV. MEASURES OF CHAOS

A. Rate of entropy increase

The Kolmogorov-Sinai (KS) entropy, equal to 1 bit per step for the classical baker's map, measures the asymptotic rate at which information about an initial phase-space point must be supplied in order to keep the ability to predict the n th iterate of the map to a given accuracy. Furthermore, if a stochastic perturbation is added to the map, the KS entropy measures the average entropy increase per step that results from averaging over the perturbation. Both of these properties are very easily understood in the shift-map representation of the map [20].

For quantum systems, a constant rate of entropy increase in the presence of environment-induced decoherence has been proposed [12,13] as a signature of chaos. This rate of entropy increase is closely related to the concept of quantum dynamical entropy [8,14]. As in the classical case, the analysis is greatly facilitated by the shift-map character of the quantum baker's map.

The entropy increase in a chaotic system is due to the exponential magnification of small-scale, local perturbations. Since perturbing all qubits in the spin chain at the same rate corresponds to a perturbation on all scales simultaneously, an entropy increase can be regarded as a signature of chaos only if the qubits are perturbed at different rates. This condition is fulfilled in our system, since the spin relaxation timescales T_2 for the hydrogen and carbon atoms in trichloroethylene differ by about one order of magnitude.

In our first proposed experiment, the system is prepared in the initial pure state

$$|\psi_0\rangle = |0_y\rangle \otimes |0_y\rangle \otimes |0_y\rangle = \frac{1}{2\sqrt{2}}(|0\rangle + i|1\rangle) \otimes (|0\rangle + i|1\rangle) \otimes (|0\rangle + i|1\rangle).
\tag{36}$$

To find the system entropy, $S(n)$, after n steps ($n = 1, \dots, 6$), the map $T_{\mathcal{M}}$ is iterated n times by applying the pulse sequences (29) and (30) alternately. The final density operator $\rho(n)$ is then measured using quantum tomography [33,10] and the entropy is determined from $S(n) = -\text{tr}[\rho(n) \log_2 \rho(n)]$. Although standard NMR techniques give one the traceless part of the density operator only, there exist methods (at least in principle) to determine $\rho(n)$ fully, as is required for determining the entropy $S(n)$. One such method is to do tomography of the quantum operation [34], where the pulse sequence is applied to different initial states.

Another possibility would be to estimate the relative size of the traceless component by measuring the signal strength.

We have simulated this experiment by numerically solving the master equation (34). The result of the simulation is shown by the data points labeled “chaotic” in Fig. 2. The data points labeled “regular” are the results of a control simulation using the regular map $T_{\mathcal{R}}$ defined in Section III F. In both cases, the entropy increases rapidly and approaches the value of 3 bits, which is the maximal von Neumann entropy in 8-dimensional Hilbert space. There is no clear difference between the regular and chaotic cases. The apparent reason is that due to the small T_2 timescales $1/\Gamma_{C_1}$ and $1/\Gamma_{C_2}$ two of the three qubits are strongly perturbed. To show that our conclusions do not depend on the assumptions leading to the simplified Hamiltonian (16), we have repeated the simulations leading to Fig. 2 using the full Hamiltonian (15). The data points labeled “regular+xy” show the result in the regular case; in the chaotic case, the extra terms in the Hamiltonian made no significant difference.

If only one qubit is strongly perturbed, however, there is a clear difference between chaotic and regular behavior. In the simulation shown in Fig. 3, both $1/\Gamma_{C_1}$ and $1/\Gamma_H$ are relatively large compared to the total delay times needed for the sequences T_{odd} and T_{even} (see Sec. III E), i.e., only the C_2 spin is strongly perturbed. These T_2 timescales cannot be achieved with the molecule trichloroethylene, but there may exist other molecules with the desired properties. In this case the “regular+xy” plot differs more than in Fig. 2, but is still clearly distinguishable from the chaotic case.

In Fig. 3, the entropy increase in the chaotic case does not have a well-defined linear regime. The reason for this is the relabeling of the qubits at each step, which was introduced in Sec. III E to reduce the complexity of the pulse sequence. At alternate steps, the strongly perturbed C_2 spin thus represents either qubit 1 or qubit 2. One could eliminate this effect by performing extra physical swap operations as described in Sec. III E. Another possibility is to introduce artificial perturbations.

One can apply an artificial perturbation to a map T by adding an extra z rotation to the least significant bit, producing the perturbed map $T' = e^{i\pi\hat{Z}_2/2}T$. At each step, one randomly chooses either the perturbed or unperturbed map. A density operator results from averaging over the two possible outcomes. This is equivalent to applying a superoperator \mathcal{P} ,

$$\mathcal{P}(\rho) = \frac{1}{2}(\rho + e^{i\pi\hat{Z}_2/2}\rho e^{-i\pi\hat{Z}_2/2}). \quad (37)$$

The results of this and the next section depend on the strength and locality of the perturbation, but are rather insensitive to its exact form. This is a general property of entropy measures for quantum chaos, which have to be defined with respect to a class of local perturbations (see, e.g., [8]). Clearly, a perturbation that commutes with the unperturbed dynamics will not reveal any chaotic properties of the latter.

To perturb the same logical qubit at even and odd steps of the map $T_{\mathcal{M}}$, we apply after each odd step the perturbation superoperator

$$\mathcal{P}_{\text{odd}}(\rho) = \frac{1}{2}(\rho + e^{i\pi\hat{Z}_H/2}\rho e^{-i\pi\hat{Z}_H/2}) \quad (38)$$

and after each even step the perturbation superoperator

$$\mathcal{P}_{\text{even}}(\rho) = \frac{1}{2}(\rho + e^{i\pi\hat{Z}_{C_2}/2}\rho e^{-i\pi\hat{Z}_{C_2}/2}) \quad (39)$$

to the density operator ρ . For the regular map $T_{\mathcal{R}}$, we apply \mathcal{P}_{odd} at each step. In an actual experiment, a convenient way of averaging over different perturbations consists in applying selected gradient fields [35].

The results are shown in Fig. 4. We have assumed large relaxation times for all three spins. The extra terms in the Hamiltonian had only a slight effect on the chaotic case, and a negligible effect on the regular case. The simulation differentiates well between the regular and chaotic cases, and the latter shows the expected linear increase in entropy, followed by saturation at 3 bits. Unfortunately, this simulation assumes possibly unrealistic relaxation times.

B. Hypersensitivity to perturbation

Hypersensitivity to perturbation is an information-theoretic criterion for classical and quantum chaos [15–17] which has been shown to be equivalent to a standard definition of classical chaos under general assumptions [16]. Suppose a system is perturbed, for instance by being acted on by an unknown force with a known distribution. Averaging over all possible perturbations causes the entropy of the state to increase. One can reduce this entropy growth by obtaining information about the perturbation, such as the actual value of the force to some precision. By having more information about the perturbation, the uncertainty in the state (and hence its entropy) decreases. To reduce the entropy growth by an average amount ΔS requires information $I \geq \Delta S$ about the perturbation. In particular, we want to know the minimum amount of information I_{min} needed to produce a given entropy reduction ΔS . A system is hypersensitive to perturbation if the information I_{min} needed to lower the system entropy increase by an average amount ΔS is very large compared to ΔS . Precise definitions of the quantities I_{min} and ΔS are given in [17]. For a general introduction, see [18].

We will show in this section that hypersensitivity to perturbation can be detected in the 3-qubit quantum baker’s map even in the presence of the actual noise levels for trichloroethylene. As in the last section, we define perturbed maps $T'_{\mathcal{R}} = e^{i\pi\hat{Z}_H/2}T_{\mathcal{R}}$ and $T'_{\mathcal{M}} = e^{i\pi\hat{Z}_H/2}T_{\text{odd}}$ or $T'_{\mathcal{M}} = e^{i\pi\hat{Z}_{C_2}/2}T_{\text{even}}$ for odd or even steps, respectively. Applying randomly at each step either the perturbed or the unperturbed map leads, after n steps, to 2^n possible different *perturbation histories*.

Due to the fast decoherence, it is necessary to limit the number of steps to $n = 3$, corresponding to $N_{\text{hist}} = 2^n = 8$ different perturbation histories. The proposed experiment is to apply, each time starting from the initial state $|\psi_0\rangle$ defined in (36), all $N_{\text{hist}} = 8$ perturbation histories, to obtain the list of final density operators $\mathcal{L} = \{\tilde{\rho}_1, \dots, \tilde{\rho}_{N_{\text{hist}}}\}$ by quantum tomography, and to analyze the distribution of the N_{hist} density operators in density operator space. We assume that, in a random trial, all N_{hist} perturbation histories would occur with the same probability $1/N_{\text{hist}}$. We can find the entropy $\bar{S}_{\text{max}} = -\text{tr}(\tilde{\rho} \log_2 \tilde{\rho})$ of the *average* density operator

$$\tilde{\rho} = \frac{1}{N_{\text{hist}}} \sum_{j=1}^{N_{\text{hist}}} \tilde{\rho}_j. \quad (40)$$

As argued in the last section, this should grow quickly with the number of iterations n . Our simulation using the relaxation times for trichloroethylene (Fig. 5) gave, for $n = 3$,

$\bar{S}_{\max} = 2.67$ bits in the chaotic case, $\bar{S}_{\max} = 2.74$ bits in the regular case, and $\bar{S}_{\max} = 2.72$ bits in the regular case with x and y terms: nearly identical values. The slightly lower entropy in the chaotic case arises because of the alternation between T_{odd} and T_{even} ; it is otherwise of no significance.

The values for the entropy increase alone, therefore, do not reveal much about the distribution of the density operators in the ensemble. In particular, they do not reveal whether the ensemble is *orthogonal* (in which case the entropy increase corresponds to purely classical information) or nonorthogonal (corresponding to quantum information). Obtaining information about which perturbation history has been realized can reduce the entropy from \bar{S}_{\max} to a lower value \bar{S} ; analyzing the dependence of $\Delta\bar{S} = \bar{S}_{\max} - \bar{S}$ on the information needed gives a measure of how nonorthogonal the ensemble is [17].

We could obtain the total possible information by determining exactly which perturbation history occurred. This corresponds to $\log_2 N_{\text{hist}} = 3$ bits of acquired information, and would reduce us from considering the average density operator $\tilde{\rho}$ to considering only a single final density operator $\tilde{\rho}_j$. However, we could also obtain *partial* information about the perturbation history by partitioning the N_{hist} final density operators into $R < N_{\text{hist}}$ groups, and determining only which group the operator was in. Since we are actually interested in the minimum information I_{\min} needed to produce a given entropy reduction, we would like to choose groupings which maximize the entropy reduction.

More precisely, consider a partitioning of the list \mathcal{L} into R groups, labeled by $r = 1, \dots, R$. We denote by N_r the number of density operators in the r th group ($\sum_{r=1}^R N_r = N_{\text{hist}}$). The N_r density operators in the r th group and their probabilities are denoted by $\rho_1^r, \dots, \rho_{N_r}^r$ and $q_1^r, \dots, q_{N_r}^r$, respectively. In our case, all $q_i^r = 1/N_{\text{hist}}$. In a random trial, the system state will be in the r th group with probability

$$p_r = \sum_{i=1}^{N_r} q_i^r = \frac{N_r}{N_{\text{hist}}} . \quad (41)$$

The knowledge that the system state is in group r is described by the density operator

$$\rho_r = p_r^{-1} \sum_{i=1}^{N_r} q_i^r \rho_i^r = N_r^{-1} \sum_{i=1}^{N_r} \rho_i^r . \quad (42)$$

We define [17] the system entropy conditional on being in group r ,

$$S_r = -\text{tr}(\rho_r \log_2 \rho_r) , \quad (43)$$

the average conditional entropy

$$\bar{S} = \sum_r p_r S_r = \bar{S}_{\max} - \Delta\bar{S} \leq \bar{S}_{\max} , \quad (44)$$

and the average information

$$I = - \sum_r p_r \log_2 p_r \geq \Delta\bar{S} . \quad (45)$$

The information I_{\min} needed about the perturbation to reduce the system entropy by an amount ΔS is now defined as the minimum of I over all groupings for which $\Delta\bar{S} \geq \Delta S$, i.e., all groupings for which the system entropy is reduced by at least ΔS .

The particular case we are treating is simple enough that we could actually try all possible groupings to find the one which minimizes I for a given ΔS . In general, however, for large numbers of iterations the number of groupings grows far too rapidly to exhaustively consider all possibilities. Instead, we must find an efficient grouping algorithm which approximates this minimum.

To find an approximation to I_{\min} as a function of ΔS , we introduce the concept of nearly optimal groupings. Given a *tolerable entropy* ΔS , we want to partition the list of density operators \mathcal{L} into groups so as to minimize the information I without violating the condition $\Delta \bar{S} \geq \Delta S$ or $\bar{S} \leq \bar{S}_{\max} - \Delta S$. To minimize I , it is favorable to make the groups as large as possible. Furthermore, to reduce the contribution to \bar{S} of a group containing a given number of density operators, it is favorable to choose density operators that are as close together as possible in some suitable sense (see below).

To find a nearly optimal grouping into R groups, we first choose R density operators at random from the list \mathcal{L} . Then for each of the remaining density operators in the list, we execute the following procedure. Let ρ_k be the next density operator in the list to be grouped, and let ρ'_i denote the average of all density operators grouped into group i so far (i.e. excluding all those that have not yet been grouped). Then ρ_k is added to that group j for which the “distance”

$$d(\rho'_j, \rho_k) = -\text{tr} \frac{1}{2}(\rho'_j + \rho_k) \log \frac{1}{2}(\rho'_j + \rho_k) - \frac{1}{2} \left[-\text{tr} \rho_k \log \rho_k - \text{tr} \rho'_j \log \rho'_j \right] \quad (46)$$

is minimal. Of course there exist many alternative grouping algorithms, of which we tried several, but the one described above gave consistently the best results (i.e., the smallest I for a given ΔS).

Figure 5 shows I_{\min} versus ΔS for both the chaotic and the regular case. The slope of the chaotic curve is roughly equal to 6, i.e., about $6n$ bits of information about the perturbation are needed to reduce the system entropy increase by n bits. In the regular case, 1 bit of information about the perturbation is sufficient to reduce the system entropy increase by almost 0.7 bits (0.5 bits with $\hat{X}\hat{X}$ and $\hat{Y}\hat{Y}$ terms). The criterion of hypersensitivity to perturbation thus differentiates well between chaotic and regular behavior. Furthermore, the slope of 6 in the chaotic case is not very far from the dimension of Hilbert space, $D = 8$. A slope close to D is characteristic for a random distribution of pure states in Hilbert space, and has been conjectured to hold for chaotic quantum systems [36]. The steep slope indicates that the ensemble is highly nonorthogonal.

V. CONCLUSION

The quantum baker’s map can be implemented with present-day technology on a 3-qubit NMR quantum computer. In order to investigate the feasibility of quantum chaos experiments using this system, we have numerically solved the master equation for the NMR system, including the Hamiltonian time evolution, the RF pulses, and phase noise due to the environment.

We have proposed and analyzed two specific quantum chaos experiments. In both experiments, we compare the quantum baker’s map with a trivial map. One experiment analyses the increase of the von Neumann entropy due to decoherence. We show that in principle

this experiment distinguishes well between the chaotic and regular cases, but a successful execution requires lower decoherence rates than seem to be achievable at present.

The second proposed experiment looks for hypersensitivity to perturbation, an information-theoretic criterion for chaos. We have shown that hypersensitivity to perturbation can be detected in the 3-qubit quantum baker's map even in the presence of the actual noise levels for trichloroethylene. Using realistic estimates for the experimental parameters, our simulations show that this criterion differentiates very well between chaotic and regular behavior.

We have thus shown that the quantum baker's map displays behavior of fundamental interest even for the 8-dimensional Hilbert space of three qubits. Quantum computers can be used to study quantum chaos under highly controlled experimental conditions.

ACKNOWLEDGMENTS

The authors profited from discussions with C. M. Caves, I. Chuang, J. A. Jones, E. Knill, R. Laflamme, M. Mosca, M. Nielsen, and W. Zurek. Funding for RS came partially from the UK's EPSRC. TAB was funded in part by NSF Grant No. PHY94-07194.

APPENDIX A:

Here we give the RF pulses corresponding to the baker's map T defined by the sequence of gates (11). This unfortunately includes interactions between non-neighboring bits. However, one can get around this problem by inserting an extra pair of swap gates S_{01} at the beginning and end of the iteration, making the gate sequence

$$T = S_{01}S_{12}A_1B_{01}^\dagger(\pi/2)B_{12}^\dagger(\pi/4)A_0S_{01}B_{12}^\dagger(\pi/2)A_2A_1B_{01}(\pi/2)A_0S_{01}. \quad (\text{A1})$$

The S_{01} gates cancel between iterations, so one need only swap at the beginning and end of the entire run; and since the labeling of bits is arbitrary, these swaps can be absorbed into the process of initial state preparation and final state tomography. Thus, for each iteration we perform the sequence of gates

$$T' = S_{12}A_1B_{01}^\dagger(\pi/2)B_{12}^\dagger(\pi/4)A_0S_{01}B_{12}^\dagger(\pi/2)A_2A_1B_{01}(\pi/2)A_0, \quad (\text{A2})$$

which only couples neighboring bits.

Here there is no need to change representation every other step, so we may fix a label onto the three bits. In this case, we will identify bit 0 with H , bit 1 with C_1 , and bit 2 with C_2 . The sequence of pulses corresponding to each gate is described in detail in section III, above. All that is required is to combine them into a pulse sequence for the entire map:

$$\begin{aligned} T' = & Y_{C_1}(\pi/2)X_H(\pi)X_{C_1}(\pi)U(4\tau)X_H(\pi)U(4\tau)Y_{C_2}(\pi/2)X_{C_2}(8\tau\delta)Y_{C_2}(8\tau\delta - \pi/2) \\ & \times X_{C_1}(\pi/2)X_{C_2}(\pi/2)U(4\tau)X_H(\pi)U(4\tau)Y_{C_1}(\pi/2)Y_{C_2}(\pi/2)X_{C_1}(\pi)X_{C_2}(\pi)U(4\tau) \\ & \times X_H(\pi)U(4\tau)X_{C_1}(-\pi/2)X_{C_2}(-\pi/2)Y_{C_1}(-3\pi/4)X_{C_1}(\pi/2)Y_{C_2}(8\delta\tau - \pi/2)X_{C_2}(-\pi/2) \\ & \times U(\tau)X_{C_2}(\pi)U(\tau)X_{C_1}(\pi/2)X_H(\pi/2)Y_H(\pi/4)X_H(\pi/2)Y_{C_1}(\pi/8)X_{C_1}(-\pi/2)U(\tau) \\ & \times X_H(\pi)U(\tau)X_{C_2}(\pi/2)Y_{C_2}(\pi/8 - 2\delta\tau)X_{C_2}(\pi/2)U(2\tau)X_{C_2}(\pi)U(2\tau)X_{C_1}(\pi/2) \end{aligned}$$

$$\begin{aligned}
& \times X_H(\pi/2)U(2\tau)X_{C_2}(\pi)U(2\tau)X_H(-3\pi/2)Y_H(-\pi/2)X_{C_1}(-3\pi/2)Y_{C_1}(-\pi/2)U(2\tau) \\
& \times X_{C_2}(\pi)U(2\tau)Y_H(\pi/2)U(2\tau)X_H(\pi)U(2\tau)Y_{C_2}(\pi/2)X_{C_2}(4\delta\tau - \pi/4)X_{C_1}(-\pi/2) \\
& \times Y_{C_1}(-\pi/4)X_{C_1}(-5\pi/4)Y_{C_1}(-\pi/2)U(3\tau)X_{C_2}(\pi)U(3\tau)Y_H(\pi/2)X_H(\pi/4), \tag{A3}
\end{aligned}$$

where the basic timescale is $\tau = \pi/4j_1 = \tau_1/2$.

REFERENCES

- [1] N. L. Balazs and A. Voros, *Ann. Phys.* **190**, 1 (1989).
- [2] M. Saraceno, *Ann. Phys.* **199**, 37 (1990).
- [3] R. Schack, *Phys. Rev. A* **57**, 1634 (1998).
- [4] N. A. Gershenfeld and I. L. Chuang, *Science* **275**, 350 (1997).
- [5] D. Cory, A. Fahmy, and T. Havel, *Proc. Nat. Acad. Sci. USA* **94**, 1634 (1997).
- [6] D. G. Cory, M. D. Price, and T. F. Havel, *Physica D* **120**, 82 (1998).
- [7] M. Mosca, (1997), unpublished note.
- [8] R. Alicki and M. Fannes, *Lett. Math. Phys.* **32**, 75 (1994).
- [9] M. Saraceno and A. Voros, *Physica D* **79**, 206 (1994).
- [10] R. Laflamme et al., *Phil. Trans. Roy. Soc. London A* **356**, 1743 (1998).
- [11] G. Lindblad, *Commun. Math. Phys.* **48**, 119 (1976).
- [12] W. H. Zurek and J. P. Paz, *Phys. Rev. Lett.* **72**, 2508 (1994).
- [13] W. H. Zurek and J. P. Paz, *Physica D* **83**, 300 (1995).
- [14] R. Alicki, D. Makowiec, and W. Miklaszewski, *Phys. Rev. Lett.* **77**, 838 (1996).
- [15] C. M. Caves, in *Physical Origins of Time Asymmetry*, edited by J. J. Halliwell, J. Pérez-Mercader, and W. H. Zurek (Cambridge University Press, Cambridge, England, 1993), p. 47.
- [16] R. Schack and C. M. Caves, *Phys. Rev. E* **53**, 3387 (1996).
- [17] R. Schack and C. M. Caves, *Phys. Rev. E* **53**, 3257 (1996).
- [18] C. M. Caves and R. Schack, *Complexity* **3**, No. 1, 46–57 (1997).
- [19] V. I. Arnold and A. Avez, *Ergodic Problems of Classical Mechanics* (Benjamin, New York, 1968).
- [20] V. M. Alekseev and M. V. Yakobson, *Phys. Reports* **75**, 287 (1981).
- [21] H. Weyl, *The Theory of Groups and Quantum Mechanics* (Dover, New York, 1950).
- [22] C. M. Caves, 1998, unpublished note.
- [23] R. Cleve, A. Ekert, C. Macchiavello, and M. Mosca, *Proc. R. Soc. Lond. A* **454**, 339 (1998).
- [24] R. Schack and T. Brun, unpublished.
- [25] E. Knill, private communication.
- [26] J. A. Jones, private communication.
- [27] I. Chuang, private communication.
- [28] J. A. Jones, R. H. Hansen, and M. Mosca, (1998), eprint quant-ph/9805070.
- [29] O. W. Sørensen *et al.*, *Progress in NMR Spectroscopy* **16**, 163 (1983).
- [30] M. Goldman, *Quantum Description of High-Resolution NMR in Liquids* (Clarendon Press, Oxford, 1988).
- [31] H. J. Carmichael, *An Open Systems Approach to Quantum Optics* (Springer, Berlin, 1993).
- [32] R. Schack and T. A. Brun, *Comp. Phys. Comm.* **102**, 210 (1997).
- [33] M. G. Raymer, M. Beck, and D. F. McAlister, *Phys. Rev. Lett.* **72**, 1137 (1994).
- [34] I. L. Chuang and M. A. Nielsen, *J. Mod. Opt.* **44**, 2455 (1997).
- [35] D. G. Cory et al., *Phys. Rev. Lett.* **81**, 2152 (1998).
- [36] R. Schack and C. M. Caves, in *Quantum Communication, Computing, and Measurement*, eds. O. Hirota, A. S. Holevo, and C. M. Caves, p. 317 (Plenum Press, New York, 1997).

FIGURES

FIG. 1. The molecule trichloroethylene.

FIG. 2. Entropy versus number of steps for the regular map $T_{\mathcal{R}}$ and the simplified baker's map $T_{\mathcal{M}}$. The decoherence times are $1/\Gamma_{C_1} = 0.7\text{s}$, $1/\Gamma_H = 4.0\text{s}$, and $1/\Gamma_{C_2} = 0.4\text{s}$, i.e., realistic values. The curve labeled “regular+xy” was generated with the XX and YY terms included in the Hamiltonian. For the chaotic map, the effect of the extra terms is negligible.

FIG. 3. Entropy versus number of steps for the regular map $T_{\mathcal{R}}$ and the simplified baker's map $T_{\mathcal{M}}$. The decoherence times are $1/\Gamma_{C_1} = 10\text{s}$, $1/\Gamma_H = 10\text{s}$, and $1/\Gamma_{C_2} = 0.2\text{s}$, i.e., idealized values. The curve labeled “regular+xy” was generated with the XX and YY terms included in the Hamiltonian. For the chaotic map, the effect of the extra terms is negligible.

FIG. 4. Entropy versus number of steps for the regular map $T_{\mathcal{R}}$ and the simplified baker's map $T_{\mathcal{M}}$ in the presence of an artificial perturbation as described in the text. The decoherence times are $1/\Gamma_{C_1} = 1/\Gamma_H = 1/\Gamma_{C_2} = 10\text{s}$, i.e., idealized values. The curve labeled “chaotic+xy” was generated with the XX and YY terms included in the Hamiltonian. For the regular map, the effect of the extra terms is negligible.

FIG. 5. Information needed about the perturbation versus entropy reduction for the regular map $T_{\mathcal{R}}$ and the simplified baker's map $T_{\mathcal{M}}$. The decoherence times are $1/\Gamma_{C_1} = 0.7\text{s}$, $1/\Gamma_H = 4.0\text{s}$, and $1/\Gamma_{C_2} = 0.4\text{s}$, i.e., realistic values. The curve labeled “regular+xy” was generated with the XX and YY terms included in the Hamiltonian. For the chaotic map, the effect of the extra terms is negligible.

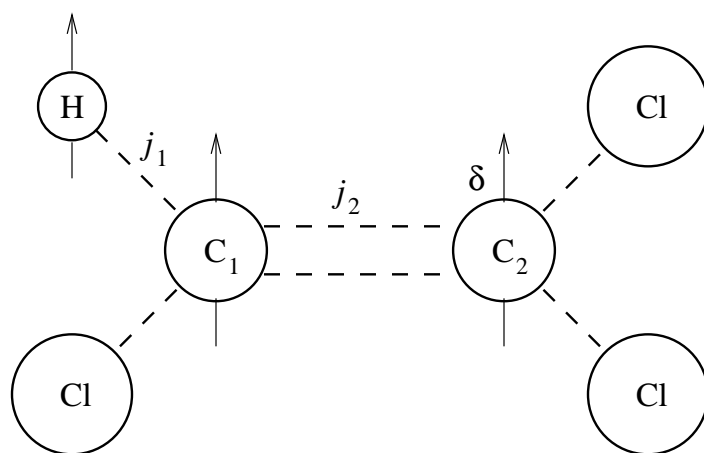


Figure 1 (Brun)

Figure 2 (Brun)

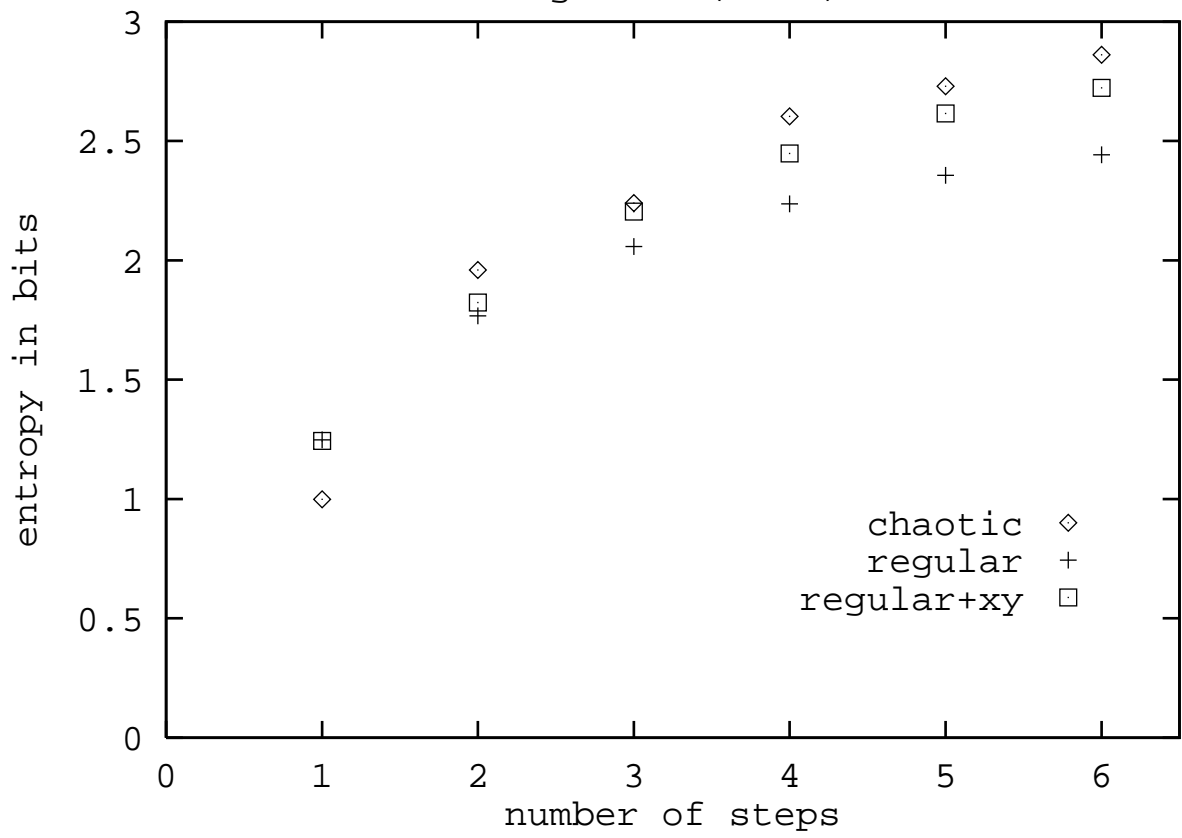


Figure 3 (Brun)

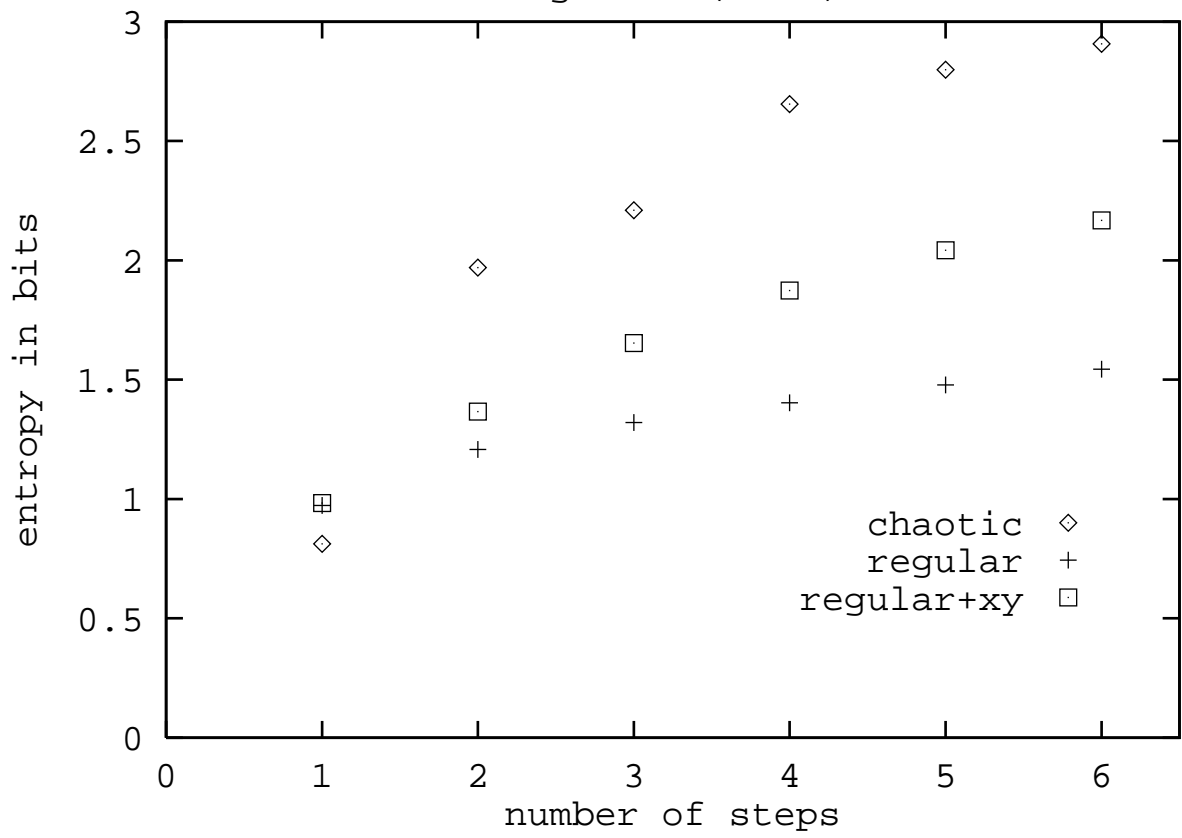


Figure 4 (Brun)

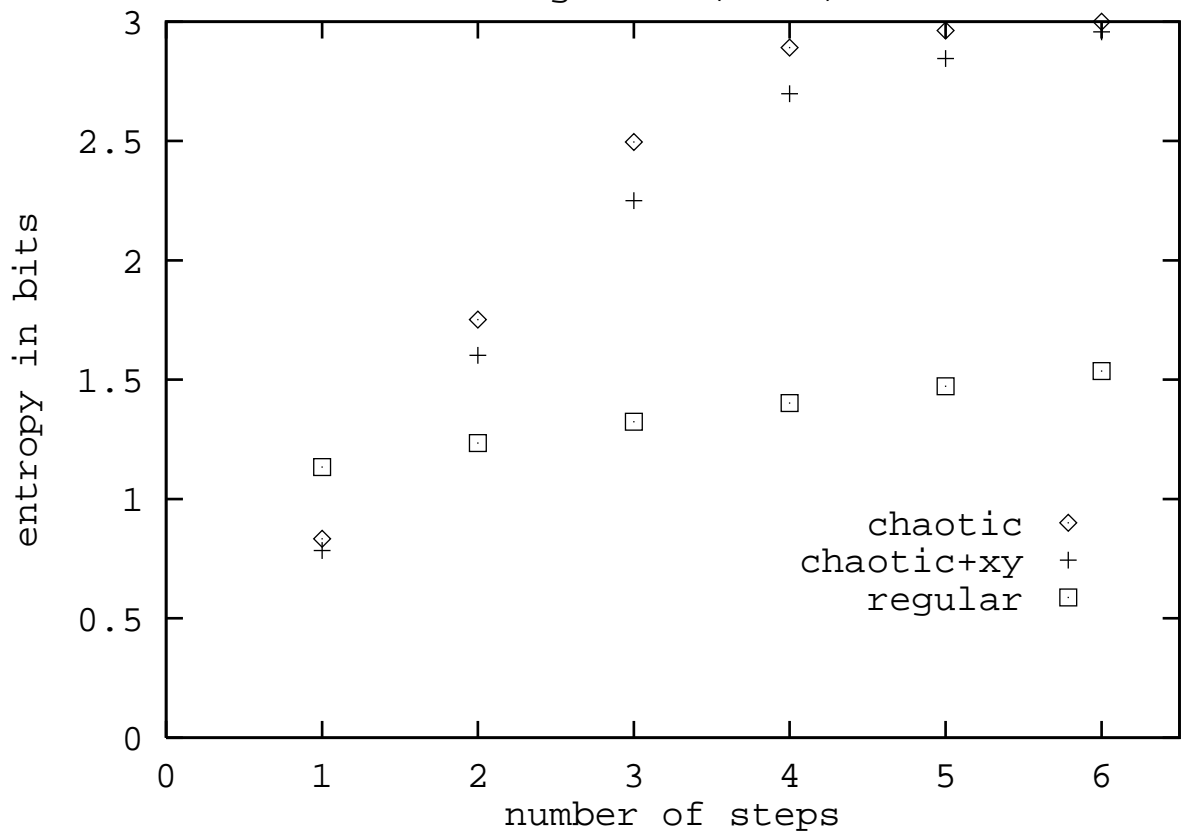


Figure 5 (Brun)

